



# Effects of Grain Size on Deformation Inhomogeneity of Hot-Deformed AA7075

B. Y. Su<sup>1,2</sup>, N. Guo<sup>1,2(✉)</sup>, B. T. Tang<sup>1,2,3</sup>, W. X. Yang<sup>1,2</sup>, G. Q. Liu<sup>1,2</sup>, and Z. Liu<sup>3</sup>

<sup>1</sup> Department of Mechanical Engineering, Qilu University of Technology (Shandong Academy of Sciences), Jinan, China

guoning19891227@163.com

<sup>2</sup> Shandong Institute of Mechanical Design and Research, Jinan 250103, China

<sup>3</sup> Jinlei Technology Co. Ltd., Jinan, China

**Abstract.** The complicated and coupled effects between dislocation and dynamic recrystallization inducing deformation inhomogeneity and further damage in the hot plastic deformation process of 7075 aluminum alloy restrict the formability of thin-wall parts for new energy vehicles. In this paper, the influence of grain size on hot deformation inhomogeneity of 7075 aluminum alloy under uniaxial tension is investigated. Then, a multiscale dislocation density based crystal plasticity model is established by considering dislocation slip. After verification, the virtual polycrystalline RVE models with different grain sizes and representative crystal orientations were constructed and embedded into crystal plasticity simulation in DAMASK via spectral method. The simulation results show that with the increase of grain size, the von Mises stress and dislocation density decreases. By introducing a proportion of Cube, Goss and other recrystallization texture, the von Mises stress is 8 MPa lower than that of random crystal orientation at the same grain size.

**Keywords:** AA7075 · grain size · crystal plasticity · DAMASK

## 1 Introduction

In view of the energy crisis and the development trend of carbon neutrality, the advantages of using lightweight high-strength aluminum alloys instead of steel as automotive panels are becoming more and more obvious [1]. However, during the hot stamping process of aluminum alloy, the complex stress state and microstructure evolution are dynamically changing, especially in the industrial hot stamping process with variable temperature and transient stamping rate. The combined effect of grain size [2] and dislocation density [3] is still unclear. Therefore, it is crucial to understand the mechanism of dislocation evolution and the influence of grain size for the design and optimization of the hot stamping process.

Tajally et al. [4] investigated the influence of strain and recrystallization conditions on the hot tensile behavior of 7075 aluminum alloy and found that the elongation rate increased significantly with the increase of recrystallization temperature. Sun et al. [5]

observed that with the increase of strain rate, the dynamic recrystallization grain gradually decreased during the hot deformation process of 7075 aluminum alloy, while the grain size increased with the increase of temperature. Tang et al. [6] established a viscoplastic model considering grain size, revealing the fracture pattern and grain size evolution during the hot stamping process of 7075 alloy. Zhao et al. [7] found that ultrafine-grained (UFG) 7075 aluminum alloy had a significant reduction in dislocation density and the hardening peak disappeared after annealing, showing higher thermal stability. Although the effects of grain size and dislocation density on strain hardening and softening have been extensively studied, they only describe the macroscopic influence on hot deformation behavior and lack in-depth investigation of their combined microscale effects.

This paper systematically investigates the effects of grain size and dislocation density on the thermal deformation non-uniformity of 7075 aluminum alloy sheets at elevated temperatures. Additionally, a crystal plasticity model based on dislocation density is established to reveal the evolution of dislocation density during the hot deformation of 7075 aluminum alloy. Subsequently, RVE models with different grain sizes are constructed and simulated using DAMASK [8] open source software, revealing the effects of grain size and dislocation density on thermal deformation non-uniformity from a microscopic perspective. This study addresses the lack of understanding of grain size and thermal forming defects in complex thin-walled structures and provides theoretical guidance for the formability of AA7075 aluminum alloy.

## 2 Experimental Procedure

### 2.1 Case Study Material

The raw material with a thickness 1.5 mm used is the AA7075-T6 thin plate produced by Southwest Aluminum Group Co. Ltd., in which the lattice structure of the base phase is a face-centered cubic structure (FCC), the chemical composition is shown in Table 1.

**Table 1.** Chemical composition of AA7075-T6 aluminum alloy (w.t./%)

Element	Zn	Mg	Ti	Fe	Cr	Cu	Mn	Si	Al
W.t	5.4	2.2	0.2	0.5	0.21	1.5	0.3	0.04	Bal

### 2.2 Hot Deformation Process and Microstructure Characterization

A laser machine was used to cut specimens in the shape of a dog bone, as shown in Fig. 1. All specimens were mechanically polished with 400- and 600- silicon sandpaper to obtain smooth edges. In order to obtain data on different grain sizes and crystal orientations, a series of isothermal uniaxial thermal tensile tests were performed on the specimens parallel to the rolling direction at 623 K, 673 K and 723 K with a strain rate of 0.01/s,

followed by quenching in water to preserve the characteristic of deformed structures at high temperatures. To meet the requirements of aluminum alloy hot stamping process in actual industrial production, Fig. 1 schematically describes the simplified HFQ (Hot Form Quench) procedure of the hot tensile experiment, which is applicable for the research in this paper.

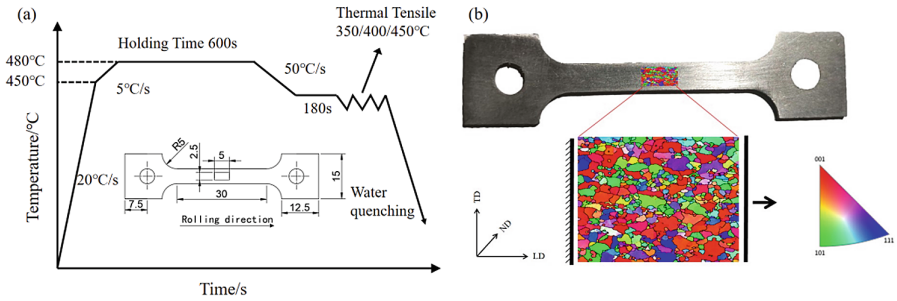


**Fig. 1.** Schematic diagram of hot tensile tests(a) and the RVE model(b).

The center position of the dog bone sample was scanned by an Oxford EBSD equipment equipped with a JSM-7900F scanning electron microscope and a working voltage of 20 kV and a scanning frequency of 550 Hz in order to calculate the grain size and analyze the crystallographic orientation. As shown in Fig. 1(b), the scanning area is  $1218 \times 837 \mu\text{m}$ . The step size is  $1 \mu\text{m}$ , and a total of 1019466 data points are obtained for each EBSD sample.

It can be seen from Fig. 2 that the overall crystal grains in the samples stretched uniaxially to fracture at different temperatures are at  $45^\circ$  to the stretching direction, and the morphology changes from equiaxed to elongated chain-like and columnar grains. As the temperature increases, the degree of recrystallization increases, and a large number of fine grains appear. With the increase of temperature and the degree of recrystallization, the average grain size at different temperatures is 25, 20, and  $15 \mu\text{m}$ , respectively.

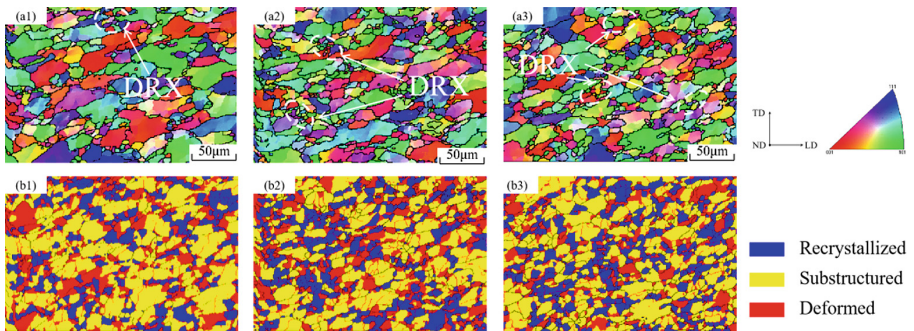


**Fig. 2.** Inverse pole figures and DRX distribution of uniaxially stretched 7075 aluminum alloy at different temperature of (a1) 623 K, (a2) 673 K, (a3) 723 K.

### 3 Crystal Plasticity Model

#### 3.1 Dislocation Density Based Crystal Plasticity Constitutive Model

This paper adopts a crystal plasticity constitutive model based on the evolution of dislocation density to define the elastic-plastic deformation behavior in a finite deformation framework. The reference shear rate for slip system  $\alpha$  is:

$$\dot{\gamma}^\alpha = \left\{ \dot{\gamma}^\alpha \exp \left[ -\frac{Q_{slip}}{k_B T} \left( 1 - \frac{|\tau^\alpha| - \tau_{pass}^\alpha}{\tau_{cut}^\alpha} \right) \right] \text{sign}(\tau^\alpha), \begin{array}{l} |\tau^\alpha| > \tau_{pass}^\alpha \\ |\tau^\alpha| \leq \tau_{pass}^\alpha \end{array} \right. \quad (1)$$

The passing stress caused by parallel dislocations is as follows:

$$\tau_{pass}^\alpha = Gb \left( \sum_{\alpha'=1}^{N_s} h^{\alpha\alpha'} (\rho^{\alpha'} + \rho_{di}^{\alpha'}) \right)^{1/2} \quad (2)$$

where  $G$  is shear modulus,  $b$  is the length of the Burgers vector for slip,  $h^{\alpha\alpha'}$  is the interaction matrix between two slip systems, and  $Q_{slip}$  is the effective activation energy of dislocation slip.

The evolution of dislocation density is closely related to the diffusion and annihilation of dislocation and the formation of dislocation dipole:

$$\dot{\rho}_{di}^\alpha = \frac{|\dot{\gamma}^\alpha|}{b\Lambda^\alpha} - \frac{2\check{d}}{b} \rho^\alpha |\dot{\gamma}^\alpha| \quad (3)$$

$$\dot{\rho}_{di}^\alpha = \frac{2(\hat{d} - \check{d})}{b} \rho^\alpha |\dot{\gamma}^\alpha| - \frac{2\check{d}}{b} \rho_{di}^\alpha |\dot{\gamma}^\alpha| \quad (4)$$

The dipole formation also decreases the mobile dislocation density. A dipole is formed if two mobile dislocations with opposite sign have a distance above  $\check{d}$ , but less than the critical radius for dipole formation,  $\hat{d}$ , see the first term in Eq. (4). The critical distance for dipole formation is defined as:

$$\hat{d} = \frac{3Gb}{16\pi|\gamma|} \quad (6)$$

$$\check{d} = D_a b \quad (7)$$

where  $D_a$  is critical distance for dislocation annihilation. In the Kocks-Mecking model, dislocation density is the primary state variable for describing the hardening behavior. Strain hardening is described here in terms of a dislocation Mean Free Path (MFP) approach, where the mean free path is denoted by  $\Lambda$ . The MFP for slip has confining contributions due to the pileup of dislocation in front of grain boundaries, dislocation-dislocation interaction, the formation of twins  $\lambda_{tw}$ , and the formation of  $\epsilon$ -martensite  $\lambda_{tr}$  is composed as:

$$\frac{1}{\Lambda_s} = \frac{1}{D} + \frac{1}{\lambda_s} + \frac{1}{\lambda_{tw}} + \frac{1}{\lambda_{tr}} \quad (8)$$

In this study, it can be simplified as follows:

$$\frac{1}{\Lambda_s} = \frac{1}{D} + \frac{1}{\lambda_s} \quad (9)$$

Among them:

$$\frac{1}{\lambda_s^\alpha} = \frac{1}{i_s} \left( \sum_{\alpha'=1}^{N_s} p^{\alpha\alpha'} (\rho^{\alpha'} + \rho_{di}^{\alpha'}) \right)^{1/2} \quad (10)$$

$D$  represents the average grain size,  $i_s$  is the fitting parameter, and  $p^{aa'}$  are coefficients that account for the interaction between dislocation on different slip systems.

### 3.2 Virtual RVE Generation

To investigate the effects of grain size and dislocation density on the thermal deformation inhomogeneity, quasi-3D RVE models with different average grain sizes were established. Considering the calculation time and result quality, the RVE consisted of  $64*64*64$  material points and was created using Dream3D software. As shown in Fig. 3, 'ET' represents the real orientation distribution function obtained from EBSD that is assigned to the material points in the RVE, while 'R' represents the RVE with orientation randomly assigned to the material points. As shown in Fig. 1(b), the RVE was subjected to thermal deformation simulation with boundary conditions.

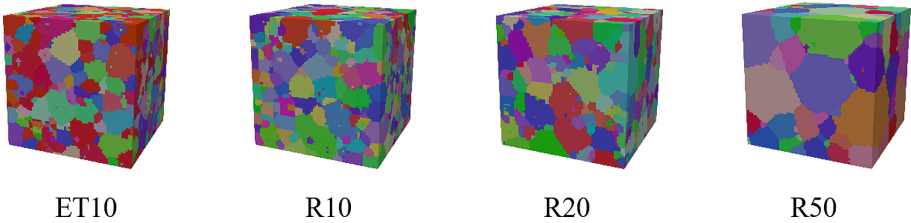
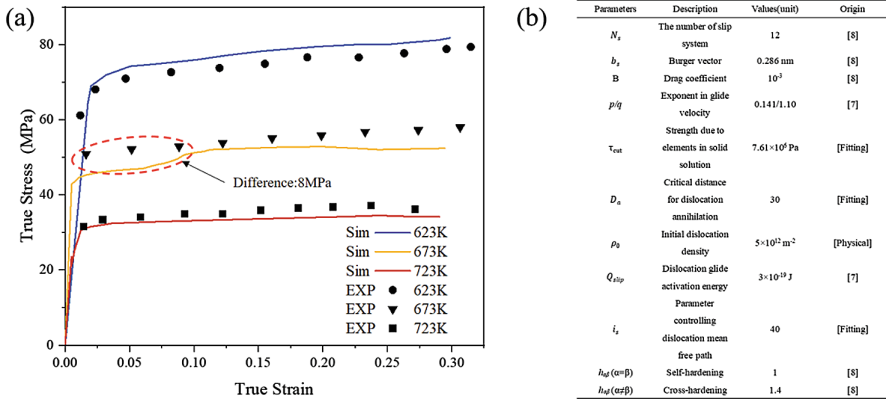


Fig. 3. IPF maps of the four generated RVEs

### 3.3 Model Verification

In Fig. 4, it can be seen that the crystal plasticity constitutive model can accurately describe the macroscopic plastic deformation behavior and mechanical response of 7075 aluminum alloy at different temperatures.



**Fig. 4.** True stress-strain curves (a) and CP parameters (b) using the RVE model and experiments with real orientation.

## 4 Discussion

### 4.1 Effect of Grain Size on Deformation Inhomogeneity

Different RVE models' stress-strain response curves under full-field crystal plasticity simulation and the distribution cloud maps of equivalent stress at 0.2 strain are shown in Fig. 5. The effect of grain size on the flow stress of AA7075 aluminum alloy plate was predicted by simulation. As shown in the figure, different grain sizes have a significant effect on the flow stress. As the grain size decreases, the simulated stress-strain response increases significantly. When the true strain is 0.2, the RVE model with an average grain size of 10  $\mu\text{m}$  and a random crystal orientation has a von Mises stress that is 10 MPa higher than the RVE model with an average grain size of 50  $\mu\text{m}$  and the same random crystal orientation. When the grain size is the same, the RVE model with the true orientation obtained from EBSD contains some recrystallized Cube and Goss textures, which are easily deformed during the deformation process, resulting in a stress-strain curve that is closer to ET10 for R20. As shown in Fig. 5(b), more stress concentration regions are generated than for the average grain sizes of 20 and 50  $\mu\text{m}$ , with stress values reaching as high as 400 MPa at the hotspots in the region. As shown in the top left curve of Fig. 5, the scattered stress concentration regions directly contribute to the increase in the model's deformation resistance.

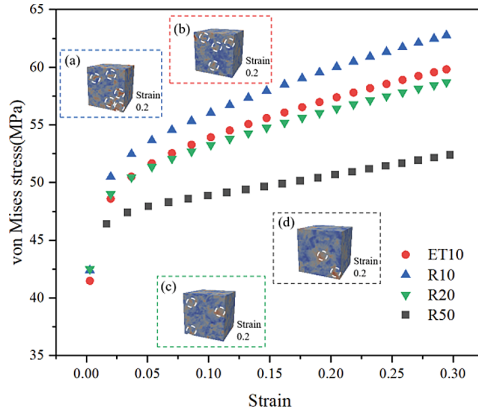


**Fig. 5.** von Mises stress evolution with different grain sizes.

## 4.2 Evolution of Dislocation Density

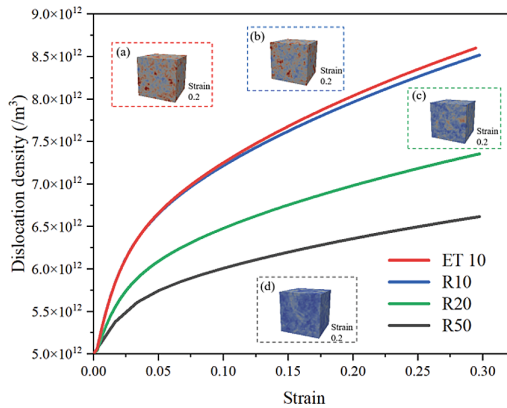


**Fig. 6.** Dislocation density evolution with different grain sizes.

In Fig. 6, it can be observed that the effect of grain size on dislocation density is much greater than the effect of crystal orientation on dislocation density. In the initial stage of hot deformation, RVEs with smaller average grain sizes have a faster increase in average dislocation density. When the degree of deformation is the same, the dislocation density of the RVE decreases as the grain size increases, as shown in Fig. 6(b) and (c). In the RVE with an average grain size of  $10\mu\text{m}$ , there are regions with higher dislocation densities, with a hot spot dislocation density of up to  $4.5 \times 10^{12}/\text{m}^2$ . Due to the smaller average grain size, there are more grain boundaries per unit volume inside the RVE, leading to the accumulation of dislocations at the grain boundaries, which hinders further hot deformation. Combined with Fig. 5, the regions of concentrated dislocation density are basically consistent with the regions of concentrated stress.

## 5 Conclusion

Different RVEs of AA7075 aluminum alloy exhibit uneven deformation during loading. The results show that with the increase of strain and grain size, the stress distribution becomes more and more inhomogeneous. At a strain of 0.2, the RVE with an average grain size of 10  $\mu\text{m}$  has a stress of 10 MPa higher than the RVE with an average grain size of 50  $\mu\text{m}$ .

During hot deformation, the dislocation density significantly decreases with an increase in average grain size, while the dislocation density growth rate is higher for smaller average grain sizes. The influence of grain size on dislocation density is far greater than that of crystal orientation. For RVEs with the same average grain size, the dislocation densities in RVEs with realistic orientations are similar to those in RVEs with random orientations.

## References

1. Abolhasani, A., Zarei-Hanzaki, A., Abedi, H.R.: The room temperature mechanical properties of hot rolled 7075 aluminum alloy. *Mater. Des.* **34**, 631–636 (2012)
2. Yang, B., Song, H., Wang, S.: Tension-compression mechanical behavior and corresponding microstructure evolution of cast A356–T6 aluminum alloy. *Mater. Sci. Eng., A* **821**, 141613 (2021)
3. Rokni, M.R., Zarei-Hanzaki, A., Roostaei, A.A.: An investigation into the hot deformation characteristics of 7075 aluminum alloy. *Mater. Des.* **32**(4), 2339–2344 (2011)
4. Tajally, M., Huda, Z., Masjuki, H.H.: Effect of deformation and recrystallization conditions on tensile behavior of aluminum alloy 7075. *Met. Sci. Heat Treat.* **53**, 165–168 (2011)
5. Sun, Z.C., Zheng, L.S., Yang, H.: Softening mechanism and microstructure evolution of as-extruded 7075 aluminum alloy during hot deformation. *Mater. Charact.* **90**, 71–80 (2014)
6. Tang, B., Li, H., Guo, N.: Revealing ductile/quasi-cleavage fracture and DRX-affected grain size evolution of AA7075 alloy during hot stamping process. *Int. J. Mech. Sci.* **212**, 106843 (2021)
7. Zhao, Y.H., Liao, X.Z., Jin, Z.: Microstructures and mechanical properties of ultrafine grained 7075 Al alloy processed by ECAP and their evolutions during annealing. *Acta Mater.* **52**(15), 4589–4599 (2004)
8. Roters, F., Diehl, M., Shanthraj, P.: DAMASK–The Düsseldorf Advanced Material Simulation Kit for modeling multi-physics crystal plasticity, thermal, and damage phenomena from the single crystal up to the component scale. *Comput. Mater. Sci.* **158**, 420–478 (2019)